ACS APPLIED MATERIALS & INTERFACES

www.acsami.org

Research Article

Inhalable siRNA Nanoparticles for Enhanced Tumor-Targeting Treatment of *KRAS*-Mutant Non-Small-Cell Lung Cancer

Guolin Zhao, William Ho, Jinxian Chu, Xiaojian Xiong, Bin Hu, Kofi Oti Boakye-Yiadom, Xiaoyang Xu,* and Xue-Qing Zhang*

Cite This: *ACS Appl. Mater. Interfaces* 2023, 15, 31273−31284

Read Online

ACCESS | Metrics & More | Article Recommendations | Supporting Information

ABSTRACT: *Kirsten rat sarcoma* (*KRAS*) is the most commonly mutated oncogene in lung cancers. Gene therapy is emerging as a promising cancer treatment modality; however, the systemic administration of gene therapy has been limited by inefficient delivery to the lungs and systemic toxicity. Herein, we report a noninvasive aerosol inhalation nanoparticle (NP) system, termed "si*KRAS*@GCLPP NPs," to treat *KRAS*-mutant non-small-cell lung cancer (NSCLC). The self-assembled si*KRAS*@GCLPP NPs are capable of maintaining structural integrity during nebulization, with preferential distribution within the tumor-bearing lung. Inhalable si*KRAS*@GCLPP NPs show not only significant tumor-targeting capability but also enhanced antitumor activity in an orthotopic mouse model of human *KRAS*-mutant NSCLC. The nebulized delivery of si*KRAS*@GCLPP NPs demonstrates potent knockdown of mutated *KRAS* in tumor-bearing lungs without causing any observable adverse effects, exhibiting a better biosafety profile than the systemic delivery approach. The results present a promising inhaled gene therapy approach for the treatment of *KRAS*-mutant NSCLC and other respiratory diseases.

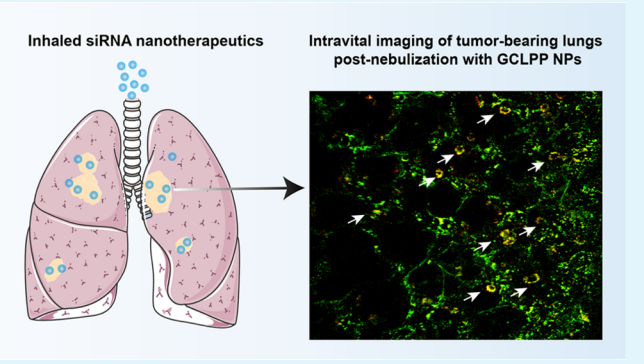

KEYWORDS: *pulmonary nucleic acid delivery, inhaled siRNA therapeutics, tumor-targeting gene therapy, KRAS mutation, lung cancer therapy*

1. INTRODUCTION

Lung cancer is one of the deadliest human cancers, causing an estimated 1.8 million deaths in 2020.[1] The complex nature of the disease and inefficient approaches to treat advanced cancer in this crucial organ system are contributors to this morbid statistic.[2] More than 85% of diagnosed lung cancer patients have non-small-cell lung cancer (NSCLC). In one-third of these NSCLC patients, the *Kirsten rat sarcoma* (*KRAS*) gene is mutated, far more frequent than other oncogenic drivers.[3−5] Mutations of *KRAS* are related to the initiation and maintenance of cancer as well as poor prognosis in patients because of the constant activation of the cell cycle, downstream proliferative pathways, and tumor plasticity due to a myriad of genomic alterations and intratumorally heterogeneity.[6−8]

The bulk of research thus far has been focused on identifying compounds that bind directly to *KRAS* and block its function.[9−15] Despite the development of several therapeutics to achieve pharmacological inhibition of *KRAS* itself, effective treatment has been elusive due to limitations, such as the inadequate response of the specific G12C inhibitor, the development of resistance to existing therapies, the absence of targeted strategies toward mutant *KRAS* mRNA, and potential toxicity to healthy tissues.[16−19] Therefore, treating *KRAS*-driven tumors effectively without systemic toxicity is a tremendous unmet clinical need.[20−22] Recently, RNA interference (RNAi), and in particular small-interfering RNA (siRNA), has shown promising antitumor efficacy with applications in *KRAS*-mutant tumors.[23,24] Selected siRNA sequence candidates should ablate multiple-mutant *KRAS* alleles without affecting the biological function of normal *KRAS* even at a low dose to minimize off-target effects and limit side effects. Note that successful delivery of therapeutics to pulmonary tumor sites is of critical importance to achieve clinically significant lung cancer therapy. Many lipid-based nanocarriers have been developed for the delivery of nucleic acids.[25−27] Despite the progress made in siRNA therapy, the majority of nanoplatforms developed for systemic administration have limited lung targeting capacity and pose potential risks of systemic toxicity.[28,29] The lack of efficient lung-targeting delivery platforms greatly limits the translation of gene therapies to a variety of pulmonary diseases.[9]

Received: April 7, 2023
Accepted: June 13, 2023
Published: June 24, 2023

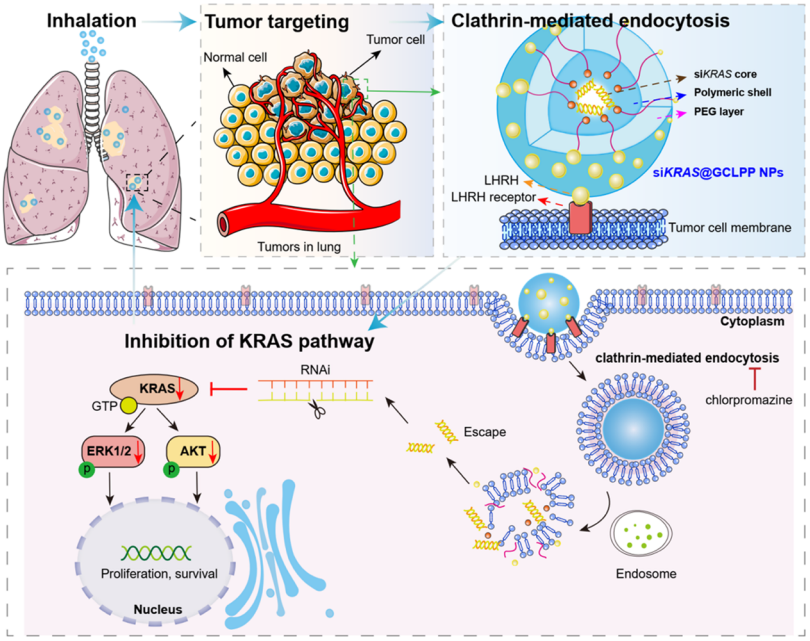

Figure 1. Schematic illustration of inhalable si*KRAS*@GCLPP NPs for suppressing *KRAS*-mutant NSCLC. The design of si*KRAS*@GCLPP NPs include (i) a cationic lipid-like molecule designated as G0-C14 entraps siRNA candidates and facilitates endosome escape,[25,30] (ii) a biodegradable PLGA-PEG acting as a matrix protecting the encapsulated siRNA during nebulization, and (iii) [D-Lys6]-LHRH conjugated to the end of the PEG molecule for binding to the LHRH receptors, which are overexpressed on the tumor cell membrane.

Compared to systemic administration, inhalation offers a more noninvasive, locally targeted administration route that bypasses liver and splenic clearance, as well as evading the mononuclear phagocyte system, which allows for more efficient uptake by the cancer cells in the lung.[9−11] We hypothesize that a delivery system that combines passive targeting through inhalation and active targeting *via* molecular recognition may offer a superior gene delivery approach. To this end, we report a novel inhalable siRNA nanotherapeutic that is engineered with luteinizing hormone-releasing hormone (LHRH) as the tumor-targeting moiety for the treatment of *KRAS*-mutant NSCLC. Specifically, we constructed the inhalable tumor-targeting NPs, termed GCLPP NPs, using three components: (i) our previously reported cationic lipid-like molecule designated as G0-C14 to entrap siRNA candidates *via* electrostatic interactions and facilitate endosomal escape of NPs;[25,30] (ii) biodegradable PLGA-PEG that acts as a matrix protecting the encapsulated siRNA during nebulization and promotes mucus penetration upon inhalation; and (iii) [D-Lys6]-LHRH conjugated to the end of the PEG molecule as targeting moiety-mediated endocytosis to cancer cells (Figure 1).[31] We chose luteinizing hormone-releasing hormone (LHRH) as the tumor-targeting ligand since tumoral LHRH receptors are specifically expressed on cancer cells, including in NSCLC.[12−15] We believe that this stepwise-targeted siRNA delivery could be a promising approach for enabling NP homing to tumor cells upon aerosol delivery of NPs to the lungs through inhalation. We investigated the antitumor efficacy of inhaled si*KRAS*@GCLPP NPs for *KRAS*-mutant NSCLC utilizing a murine orthotopic model of lung cancer. Our findings suggest that inhaled si*KRAS*@GCLPP NPs can deliver equivalent effectiveness compared to intravenously injected (IV) NPs while reducing the adverse effects associated with systemic administration. To the best of our knowledge, there have been few studies similar to the one we reported here, as most of the existing studies have employed xenograft models to explore various tumor types and have attempted to achieve targeted delivery through systemic administration.[32−34] This work presents a new avenue for noninvasive aerosol siRNA delivery that holds tremendous potential for treating *KRAS*-mutant NSCLC and other respiratory diseases.

2. RESULTS AND DISCUSSION

2.1. Characterization of siRNA@GCLPP NPs for Nebulized Delivery. LHRH decapeptide (Gln-His-Trp-Ser-Tyr-DLys(D-Cys)-Leu-Arg-Pro-NHEt) with a terminal reactive amino group on the side chain of the lysine at position 6 was covalently attached to PLGA-PEG (Figure S1). The nanoparticles were prepared *via* a self-assembly nanoprecipitation approach.[4] The cationic lipid-like compound G0-C14 developed by our group was used to entrap the siRNA molecules through electrostatic interaction. Figure 2A shows that G0-C14 could effectively condense siRNA at a weight ratio of 10 or above. Both GCLPP NPs and GCPP NPs were prepared at a G0-C14/siRNA weight ratio of 20 using the nanoprecipitation method. As shown in Figure 2B, the GCPP NPs or GCLPP NPs were stable with 170−200 nm in the size with pH ranging from 4 to 9, and the size slightly decreased under pH = 3 with GCPP NPs ∼140 nm and GCLPP NPs ∼130 nm. The average surface charge measured by dynamic light scattering (DLS) was near-neutral (−4.88−1.57 mV for GCPP NPs; −6.83−1.21 mV for GCLPP NPs). These data suggested that regardless of pH environment, GCPP NPs and GCLPP NPs could maintain a relatively intact structure. Transmission electron microscopy (TEM) showed that the spherical morphology of GCLPP NPs and GCPP NPs remained stable before (BF) and after nebulization (AF) (Figure 2C), in accordance with the size measured by DLS (Figure 2D). The particle diameters and size distribution were measured to be 168.2 and 164.8 nm for BF and AF of GCPP

https://doi.org/10.1021/acsami.3c05007
ACS Appl. Mater. Interfaces 2023, 15, 31273−31284

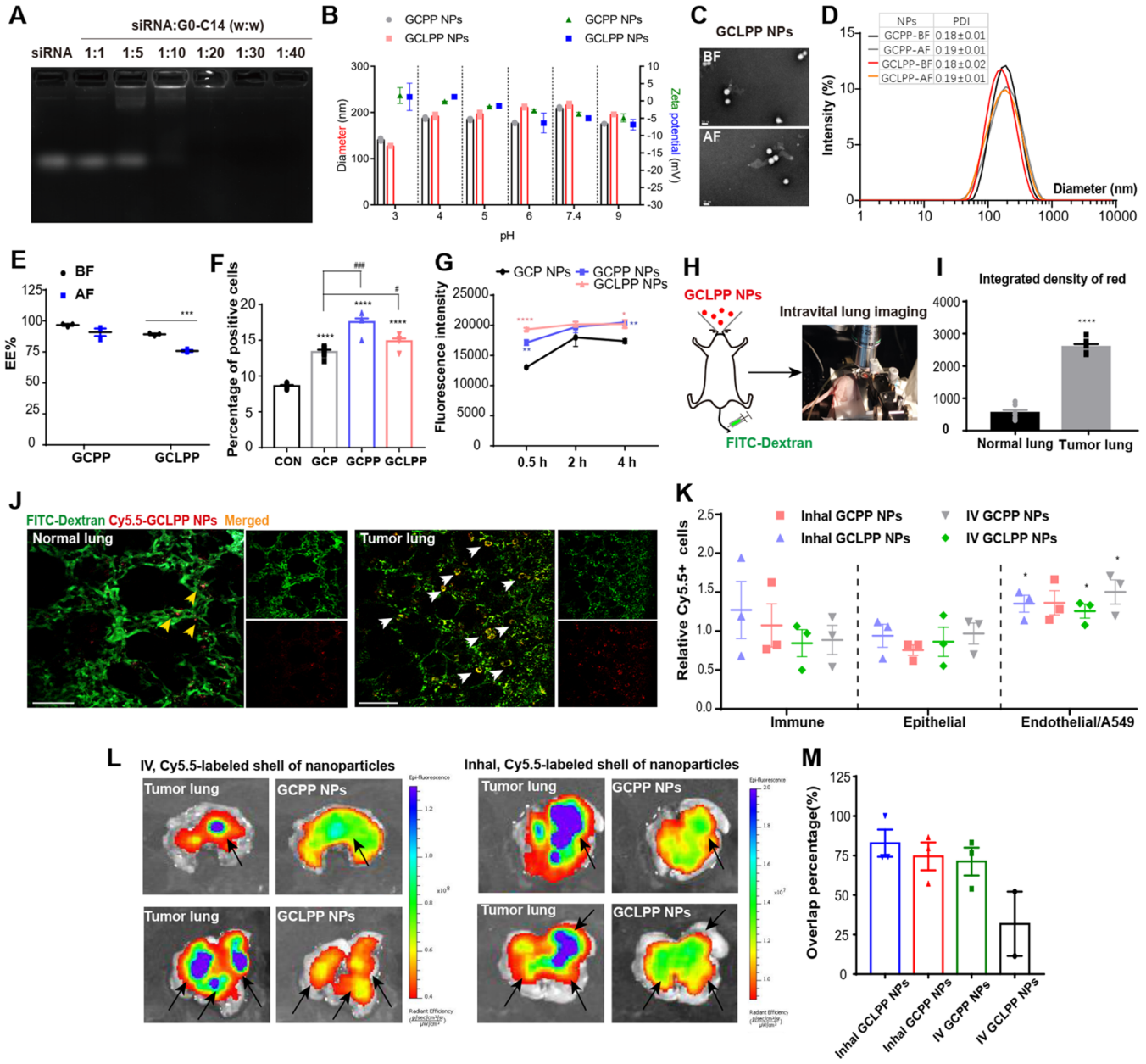

Figure 2. Characterization of LHRH-polymer/G0-C14 hybrid (GCLPP) NPs. (A) Agarose gel electrophoresis assay of siRNA stability in an organic solvent, naked siRNA, or complexed with different weight ratios of cationic G0-C14 from 1:1 to 1:40. (B) Stability of siRNA@G0-C14 nanoparticles, with or without LHRH coating, was determined by measuring the size and ζ potential in different pH environments. A weight ratio of 1:20 for siRNA to G0-C14 was used for GCPP NP and GCLPP NP preparation. (C) TEM images of GCLPP NPs before (BF) and after (AF) nebulization. Scale bar, 50 nm. (D) Nanoparticle size distribution of siRNA@GCPP NPs and GCLPP NPs before (BF) and after (AF) nebulization. (E) Encapsulation efficiency (EE%) of GCPP NPs and GCLPP NPs. ***$p < 0.001$ by unpaired two-tailed *t*-test compared to the before (BF) nebulization group. (F) Transfection effect of Cy7-siRNA encapsulated into NPs with PEG (GCPP NPs and GCLPP NPs) and without PEG (GCP NPs) in primary nasal mucosal cells. ****$p < 0.0001$ by unpaired two-tailed *t*-test compared to the control (CON) group. $^{\#}p < 0.05$ and $^{\#\#\#}p < 0.001$ compared to the GCP NP group. (G) Penetration of NPs with PEG coating (Cy5-siRNA@GCPP NPs, Cy5-siRNA@GCLPP NPs) and without PEG coating (Cy5-siRNA@GCP NPs). PEG was assessed in an artificial mucus model. *$p < 0.05$, **$p < 0.01$, ****$p < 0.0001$ compared to the GCP NP group. (H) Illustration of intravital lung imaging and (I) integrated intensity of Cy5.5-GCLPP NP signals (red) in pulmonary microcirculation in the normal lung and the tumor-bearing lung (tumor lung) tissues, and (J) the representative images are shown. ****$p < 0.0001$ by unpaired two-tailed *t*-test compared to the normal lung group. Scale bar, 100 μm. (K−M) Human A549-luc lung tumor-bearing mice were treated with Cy5.5-labeled PLGA-PEG nanoparticles, with or without LHRH coating, *via* IV injection or inhalation. The dose of injection or inhalation was 0.8 mg siRNA/kg body weight, and lung tissues were collected and imaged 2 h after administration. (K) Lungs expressing Cy5.5 fluorescence were analyzed by flow cytometry using markers for endothelial and A549 cells (CD31), epithelial (EpCAM), and immune (CD45) cells. (L) Representative images and (M) the percentage of NP fluorescence overlaid within the tumor region was analyzed by ImageJ software. *$p < 0.05$ by unpaired two-tailed *t*-test compared to the control group.

NPs and 146.7 and 156.1 nm for BF and AF of GCLPP NPs, with polydispersity (PDI) values 0.18−0.19 for GCPP NPs and 0.18−0.19 for GCLPP NPs (Figure 2D), respectively. The RiboGreen method was used to measure the change of

https://doi.org/10.1021/acsami.3c05007
ACS Appl. Mater. Interfaces 2023, 15, 31273−31284

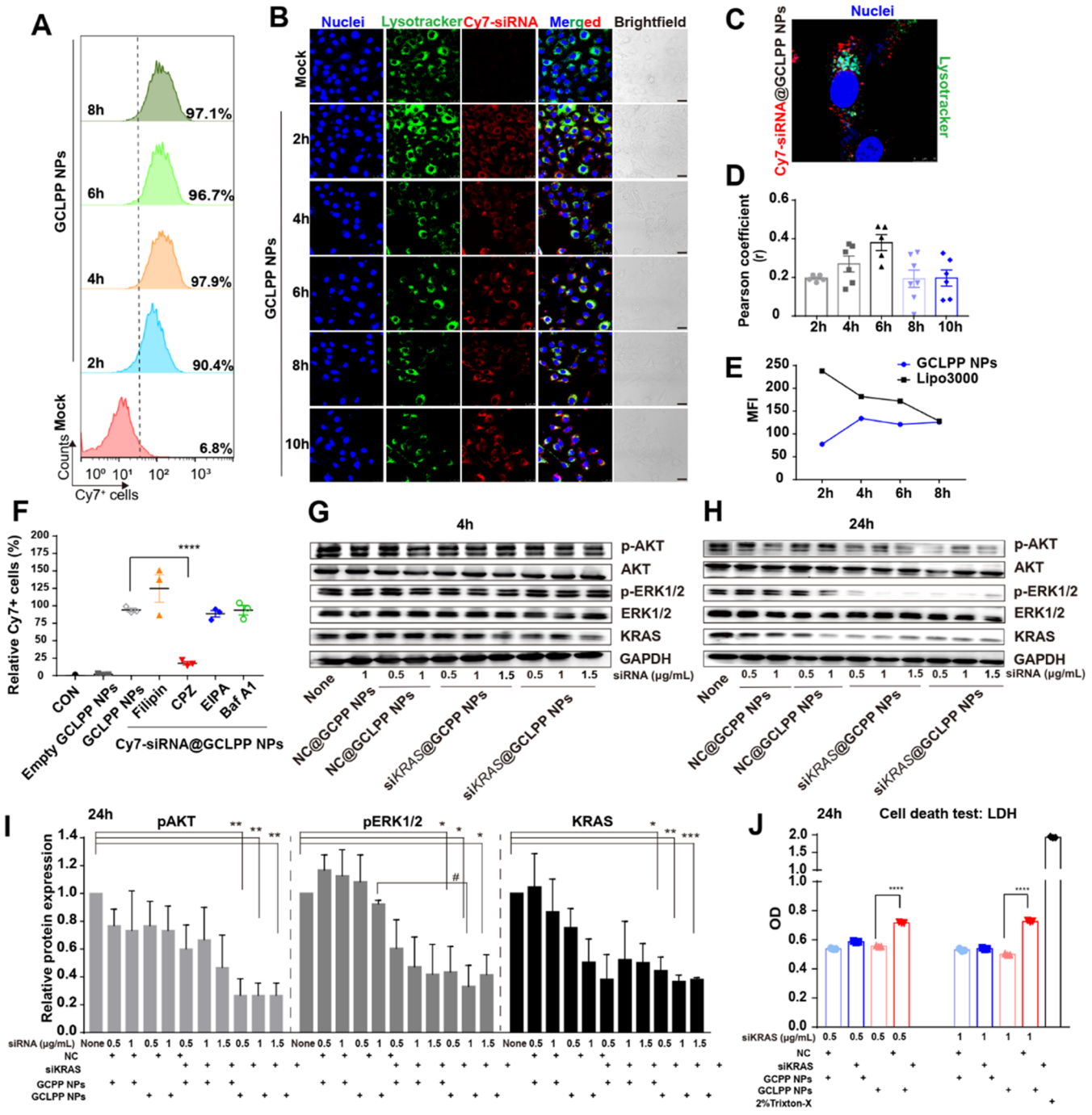

Figure 3. Endosomal escape, transfection efficiency, and inhibition of KRAS pathway by Cy7-siRNA@GCLPP NPs in the *KRAS*-mutant cell line A549 ($KRAS^{G12S}$). Cells were treated with 1 μg/mL of Cy7-siRNA@GCLPP NPs for 4 h and then incubated in standard cell culture medium. (A) Transfection efficiencies of Cy7-siRNA@GCLPP NPs evaluated by flow cytometry. (B) Subcellular localization of Cy7-siRNA of GCLPP NPs at different time points. Scale bar, 25 μm. (C) A zoomed-in picture of subcellular localization of Cy7-siRNA@GCLPP NPs at 4 h. (D) Colocalization ratio of Cy7-siRNA and Lysotracker Green-stained endosomes analyzed using ScatterJ software. (E) Mean fluorescence intensities (MFIs) of Cy7-siRNA@GCLPP NPs and Cy7-siRNA@Lipo3000. (F) Mechanism of cellular uptake and endosome escape of siRNA@GCLPP NPs in A549 cells. Prior to transfection with Cy7-siRNA@GCLPP NPs, the cells were pretreated for 30 min with serum-free medium containing inhibitors (filipin, chlorpromazine (CPZ), EIPA, and Baf A1 were used to inhibit caveolae-mediated endocytosis, clathrin-mediated endocytosis, micropinocytosis, and intracellular proton-pump effects, respectively). After 4 h of transfection, the transfection efficiency (percentage of Cy7-positive cells) was determined using flow cytometry. ****$p < 0.0001$ by unpaired two-tailed *t*-test compared to the Cy7-siRNA@GCLPP NP group. Cells were treated with increasing concentrations of NC or si*KARS via* GCPP NPs or GCLPP NPs for (G) 4 h and (H and I) 24 h. Relative protein expressions of pAKT, pERK1/2, and KRAS (from left to right) were displayed in C. *$p < 0.05$, **$p < 0.01$, ***$p < 0.001$ by unpaired two-tailed *t*-test compared to the control group (none). # $p < 0.05$ compared to the NC group. (J) Cell death was assessed using LDH tests. Scrambled siRNA served as the negative control (NC), and 2% Triton-X served as the positive control. ****$p < 0.0001$ by unpaired two-tailed *t*-test compared to the NC group.

https://doi.org/10.1021/acsami.3c05007
ACS Appl. Mater. Interfaces 2023, 15, 31273−31284

encapsulation efficiency (EE) before and after nebulization. The results showed that both GCPP and GCLPP maintained more than 75% encapsulation efficiency before and after nebulization (Figure 2E).

Nasal mucosal barrier crossing is the first barrier for nanoparticles to enter the lung tissue. To evaluate the enhanced ability to penetrate the nasal mucosal barrier, Cy7-siRNA was encapsulated in non-PEG-modified GCP NPs, and PEG-modified GCPP NPs and GCLPP NPs. The results showed that both PEG-modified GCPP NPs and GCLPP NPs exhibited higher transfection efficiency than non-PEG-modified GCP NPs in primary nasal mucosal cells. (Figure 2F). An *in vitro* artificial mucosal model was used to further evaluate the penetration ability of the candidate nanocarriers. The results showed that both the PEG-containing nanoparticles GCPP NPs and GCLPP NPs achieved higher mucosal penetration effects compared with non-PEG-modified GCP NPs (Figure 2G), which is consistent with one recent report that high PEG molarity helps lipid nanoparticles survive intact from shear forces.[31,35]

To track the cellular dynamics of inhaled siRNA@GCLPP NPs in the pulmonary circulation *in vivo*, a custom-made intravital video-rate laser scanning confocal microscopy system was used. A brief illustration of the experiment is shown in Figure 2H. FITC-dextran (green) was used to mark the capillaries and blood vessels in the lung. As shown in Figure 2J, tumor regions characterized by discontinued and cluttered vessels are observed in lung sections of the tumor-bearing mice, while normal tracheobronchial tissues obtained from healthy nu/nu mice displayed an intact and organized pulmonary vessel structure. The intravital images illustrate that more inhaled GCLPP NPs deposit in the tumor areas, exhibiting approximately a 4.8-fold higher NP fluorescence signal intensity than in normal lung tissues (Figure 2I,J). These results demonstrate that siRNA@GCLPP NPs are widely and robustly distributed in the alveoli and small conducting airways of the tumor-bearing lung *via* inhalation, suggesting that si*KRAS*@GCLPP NPs are preferentially taken up by lung tumor cells.

To evaluate the biocompatibility and safety of GCLPP NPs, a hemolysis test was conducted. Our results showed that siRNA@GCLPP NPs (1 μg siRNA/mL) did not cause hemolysis (Figure S3). Then, we compared the *in vivo* performance of siRNA@GCLPP NPs with siRNA@GCPP NPs in an orthotopic mouse model of human NSCLC. Briefly, we inoculated 5×10^6 A549 ($KRAS^{G12S}$) cells into the lungs of nu/nu mice intratracheally and then administered the nanoparticles either by intravenous injection (IV) or by inhalation *via* a nose-only chamber (inhaler). We measured NP uptake by lung cell populations after inhalation of Cy7-labeled si*KRAS* (termed Cy7-si*KRAS*@GCLPP NPs) using markers for endothelial and A549 cells (CD31)[36] and epithelial (EpCAM) and immune (CD45) cells, respectively. The flow cytometry results indicate that lung endothelial cells and A549 cells are the predominant subtypes that uptake Cy7-si*KRAS*@GCLPP NPs, with more endothelial and A549 cells expressing the Cy7 signal compared with epithelial and immune cells (Figure 2K). To determine the targeting effect, we calculated the colocalization ratio of tumor signals and fluorescence signals, as shown in Figure 2L,M. As expected, inhalation of GCLPP NPs prepared using Cy5.5-labeled PLGA-PEG resulted in higher fluorescence intensity within the tumor sites of lung tissues, in comparison with the GCPP NPs administered *via* intravenous injection (83.63 ± 33.74 *vs* 31.80 ± 28.85) or inhalation (82.80 ± 14.90 *vs* 74.72 ± 15.57). The biodistribution of Cy7-si*KRAS*@GCLPP NPs following inhalation has been investigated, as depicted in Figure S4. We observed a substantial accumulation of Cy7-si*KRAS*@GCLPP NPs in livers and kidneys, which aligns with their role as primary sites for drug metabolism and elimination (Figure S4). These findings are consistent with previous reports.[37]

The data show that the design of GCLPP NPs enables characteristics such as self-assembly, biophysical stability, and mucosal penetration effects to reach deep lung tumors for nebulized pulmonary siRNA delivery. In addition, the GCLPP NPs demonstrate biocompatibility and safety as a gene therapy delivery system.

2.2. Intracellular Trafficking and Signal Transduction Pathways of si*KRAS*@GCLPP NPs. siRNA@GCLPP NPs are synthesized using a nanoprecipitation approach in which the siRNA is encapsulated within the nanoparticle by means of electrostatic interaction. Besides siRNA encapsulation, the cellular uptake of NPs and escape from the endocytic pathway are also essential for siRNA delivery.[38] Cy7-siRNA was used to track the internalization and intracellular trafficking of siRNA@GCLPP NPs in the A549 cell line (LHRH-receptor-positive human NSCLC with $KRAS^{G12S}$). Nonviral gene delivery carriers have been extensively investigated in lung cancer but provide only variable siRNA transfection efficacy of around 40−80% in lung cancer cells.[39−43] As shown in Figure 3A, the Cy7-siRNA@GCLPP NPs showed a high transfection efficiency of above 90% in A549 cells, which was proportional to the incubation time. It was observed that 2−6 h after the transfection, Cy7-siRNA@GCLPP NPs entered the cells and were partially engulfed by endosomes or lysosomes (Figure 3B,D). A zoomed-in picture of subcellular localization of Cy7-siRNA of GCLPP NPs at 4 h is shown in Figure 3C. At 8−10 h after transfection, most of the NPs escaped from the endosomes and lysosomes and displayed a colocalization ratio of about 26% between Cy7-siRNA and lysosome/endosome (Figure 3D). Unlike the commercial transfection agent Lipofectamine 3000 (Lipo 3000), the mean fluorescence intensities (MFIs) of Cy7-siRNA@GCLPP NPs increased with the extension of transfection time, suggesting the accumulation of siRNAs in the cytoplasm (Figure 3E).

To evaluate the cellular uptake mechanism and intracellular transport of siRNA@GCLPP NPs, we pretreated A549 cells with different inhibitors. The results showed that the transfection of GCLPP NPs was not affected by a caveolae-mediated inhibitor, filipin, a macropinocytosis inhibitor, 5-(*N*-ethyl-*N*-isopropyl)-amiloride (EIPA), or a proton-pump inhibitor, bafilomycin A1 (Baf A1), but was affected by a clathrin-mediated endocytosis inhibitor (chlorpromazine) (Figure 3F). These data demonstrate that our siRNA delivery system exhibits high transfection efficiency *via* clathrin-mediated endocytosis and effective cytoplasmic escape in the A549 cell line.

After a successful escape from endosomes or lysosomes, siRNAs will enter the endogenous microRNA pathway at different stages but ultimately utilize the same conserved mechanism to downregulate target genes. The si*KRAS* candidates were designed from top-scoring sensor shRNA sequences of *KRAS* selected using a bioinformatics prediction and "sensor rules" that acquire shRNA-specific features.[23,44,45] si*KRAS* candidates were screened by measuring knockdown efficiency *via* RT-PCR in A549 cells.[23] si*KRAS*-2 was chosen

https://doi.org/10.1021/acsami.3c05007
ACS Appl. Mater. Interfaces 2023, 15, 31273−31284

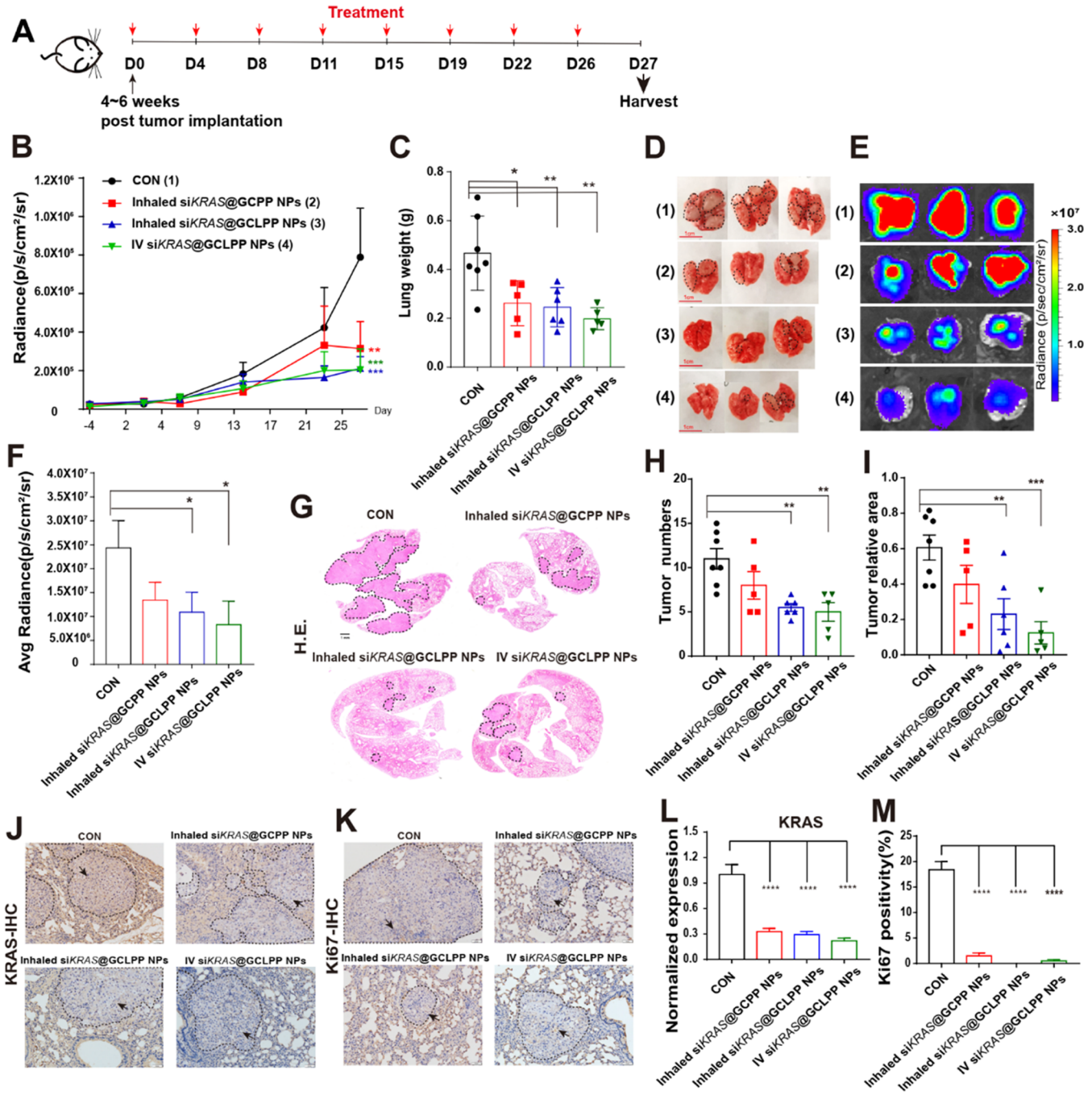

Figure 4. Inhibition of the growth of *KRAS*-mutant lung tumors in nu/nu mice with an orthotopic model of human NSCLC. Female nu/nu mice were implanted orthotopically with 5×10^6 A549-luc cells by intratracheal instillation. After four to six weeks, the lung tumors were confirmed by visualizing bioluminescence imaging (BLI) signals in the chest, then the mice were treated with inhaled si*KRAS*@GCPP NPs, inhaled si*KRAS*@GCLPP NPs, and intravenous injection (IV) si*KRAS*@GCLPP NPs at the same dose of 0.8 mg siRNA/kg, respectively. (A) Schematic illustration depicting the design of animal experiments. (B) Quantitative BLI light intensity of the chest before and after the treatment. (C) Lung weights were measured. (D) Representative photos of the lung collected from mice after indicated treatments on day 27. (1) Control group; (2) inhaled si*KRAS*@GCPP NP group; (3) inhaled si*KRAS*@GCLPP NP group; and (4) IV si*KRAS*@GCLPP NP group. Black dashed line circles indicate tumors. (E) *Ex vivo* lung BLI images representing each treatment group on day 27. (F) Quantitative BLI light intensity of *ex vivo* lung tissues on day 27. (G) H&E images from control (CON) and treatment groups are shown. Scale bar, 1 mm. (H) Tumor numbers were counted under a microscope and (I) tumor relative area (tumor area/total area) was quantified using ImageJ software. Tumor sites, indicated by black arrowheads, were analyzed by immunohistochemistry for (J, L) KRAS and (K, M) Ki67 levels. Black dashed line circles indicate tumors. Scale bar, 50 μm. Data were shown as mean ± standard error of the mean (S.E.M.) of $n = 5-7$ biologically independent mice. $^*p < 0.05$, $^{**}p < 0.01$, $^{***}p < 0.001$, $^{****}p < 0.0001$ by unpaired two-tailed *t*-test compared to the control group (CON).

for further study as it significantly decreased the mRNA levels of *KRAS* to 10% compared to the control group (Figure S2a). Additionally, si*KRAS*@GCLPP NPs exhibited superior mRNA knockdown of endogeneous *KRAS* in cancer cells compared to Lipo 3000 (Figure S2b). It is important to note that si*KRAS*@

https://doi.org/10.1021/acsami.3c05007
ACS Appl. Mater. Interfaces 2023, 15, 31273−31284

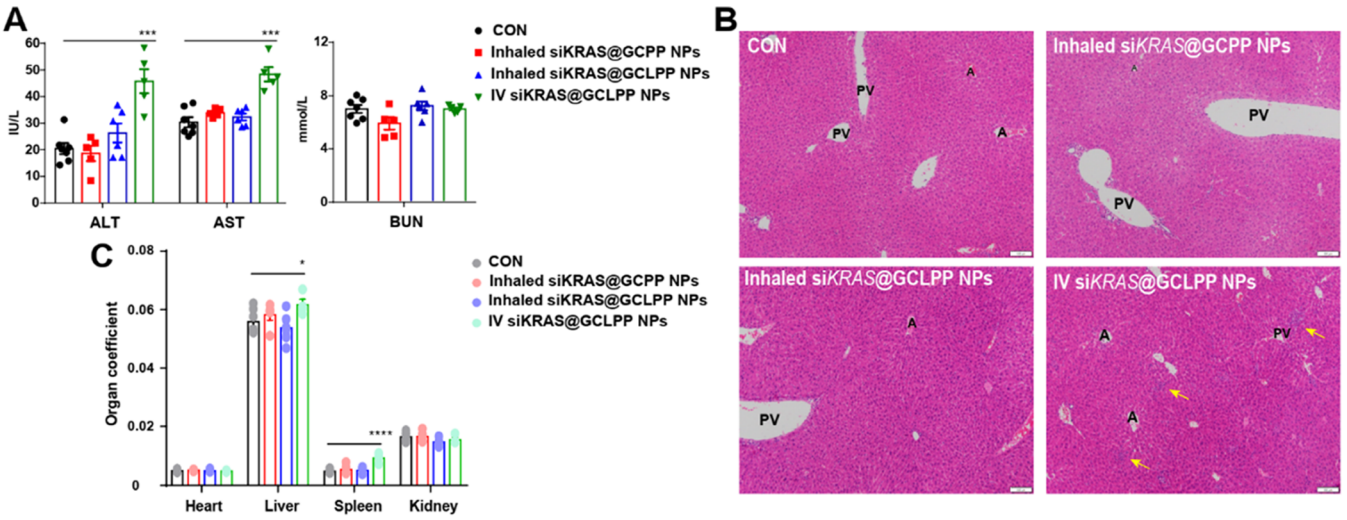

Figure 5. Toxicological profile of serum biochemistry and histology of livers after treatment on day 27. (A) Alanine aminotransferase (ALT) and aspartate aminotransferase (AST) are biomarkers for liver function. BUN (blood urea nitrogen) is a biomarker for kidney function. (B) H&E staining of livers. Yellow arrowheads showed the inflammation area. (C) Organ coefficient of main organs. *$p < 0.05$, ***$p < 0.001$, ****$p < 0.0001$ by unpaired two-tailed t-test compared with the control group (CON). PV, portal vein; A, artery. Scale bar, 100 μm.

NPs or si*KRAS*@GCLPP NPs have no observable effect on A549 cell viability in comparison to the control (Figure S2c).

Next, we investigated the potential mechanisms of inhibiting of the proliferation pathways by si*KRAS* and scrambled siRNA (negative control, NC) *via* GCPP NPs or GCLPP NPs. Oncogenic KRAS has the ability to activate various downstream effector pathways, the best characterized of which are the phosphatidylinositol 3-kinase (PI3K)/AKT and mitogen-activated protein kinase (MAPK) pathways.[19] Ultimately, these two pathways regulate cell proliferation and survival.[22] Western blotting showed that si*KRAS*@GCLPP NPs at a concentration as low as 0.5 μg/mL could effectively decrease the level of KRAS protein, resulting in a noticeable time-dependent decrease in phospho-AKT and phospho-ERK1/2 (Figure 3G−I). To confirm the impact of si*KRAS* on cell death, cells were treated with si*KRAS* and NC *via* GCPP NPs or GCLPP NPs for 24 hours. LDH tests were performed to measure cell death according to the manufacturer's instructions. Results showed a significant increase in cell death in the si*KRAS*@GCLPP NP group compared to the NC@GCLPP NP group (Figure 3J). These results demonstrate the efficacy of si*KRAS*@GCLPP NPs in reducing KRAS expression and suggest that A549 cells may serve as useful indicators of growth effects for further *in vivo* assessment.

2.3. Treatment of *KRAS*-Mutant-Selective Tumor *In Vivo* and Toxicological Evaluation. We next evaluated the antitumor activity of si*KRAS*@GCLPP NPs in female nu/nu mice with an orthotopic model of human NSCLC. After confirming the successful establishment of the tumor model after four to six weeks by *in vivo* bioluminescence imaging, treatment with si*KRAS*@GCPP NPs or si*KRAS*@GCLPP NPs was administered twice a week (Figure 4A). Tumor growth was monitored weekly by *in vivo* luciferase imaging until day 27. No significant changes in body weight were observed in the inhaled si*KRAS*@GCPP NPs and inhaled si*KRAS*@GCLPP NP groups throughout the whole treatment period. A transient decrease of body weight was observed in the IV si*KRAS*@GCLPP NP group after the 2nd dose but recovered before the 3rd dose (Figure S5). The tumor growth-suppressive effects of si*KRAS* treatment started after the second week of treatment. Quantitative analysis of bioluminescence signals demonstrated a slowing of tumor development after four weeks of treatment with inhaled si*KRAS*@GCPP NPs ($p < 0.01$), inhaled si*KRAS*@GCLPP NPs ($p < 0.001$), and IV si*KRAS*@GCLPP NPs ($p < 0.001$), as shown in Figure 4B. Lung weights revealed a significant suppression in inhaled si*KRAS*@GCPP NPs ($p < 0.05$), inhaled si*KRAS*@GCLPP NPs ($p < 0.01$), and IV si*KRAS*@GCLPP NPs ($p < 0.01$) groups on day 27 (Figure 4C,D). Correspondingly, *ex vivo* lung bioluminescence imaging (BLI) images at day 27 are displayed in Figure 4E, and quantitative analysis of BLI proved strong inhibition of tumors in the lung at the experimental endpoint (Figure 4F), especially in the inhaled si*KRAS*@GCLPP NP group ($p < 0.01$) and IV si*KRAS*@GCLPP NP group ($p < 0.01$). We also performed a histology examination to determine the overall tumor burden in the lung. H&E staining of the whole lung with tumors showed a decrease in tumor numbers as well as tumor relative areas (tumor area/total area) in the treatment groups significantly in si*KRAS*@GCLPP NP inhalation ($p < 0.01$) and si*KRAS*@GCLPP NP injection groups ($p < 0.01$) (Figure 4G). These results demonstrate that si*KRAS*@GCLPP NPs achieve significant inhibition of *KRAS*-mutant lung tumor growth in the mouse model of NSCLC.

To evaluate the effects of si*KRAS* inhibition on tumor tissue, immunohistochemistry (IHC) with a KRAS-specific antibody was performed on tumor tissue sections. Image analysis software was used to calculate the KRAS expression on tumor areas. It was shown that there was decreased KRAS staining in the tumor sites in the inhaled si*KRAS*@GCPP NP group ($p < 0.01$), the inhaled si*KRAS*@GCLPP NP group ($p < 0.01$), and the IV si*KRAS*@GCLPP NP group ($p < 0.01$) compared to the control group (Figure 4J,L). Having shown the effects of KRAS silencing on lung tumor cells, IHC staining for Ki67, a marker for dividing cells, was performed to assess the antiproliferation effects (Figure 4K,M). The quantification of this marker staining showed that the percentages of Ki67 positivity in the inhaled si*KRAS*@GCPP NP group, the inhaled si*KRAS*@GCLPP NP group, and the IV si*KRAS*@GCLPP NP group were significantly reduced compared to the control group. These results confirm that the regression of the tumors

https://doi.org/10.1021/acsami.3c05007
ACS Appl. Mater. Interfaces 2023, 15, 31273−31284

owing to the efficient silencing of *KRAS* ultimately leads to a strong inhibition of the proliferation of tumor cells.

Systemic toxicity is an important consideration in drug development, as it can limit the therapeutic potential of a drug and may lead to adverse effects in patients. Considering that the liver and kidney are the two main organs, which metabolize siRNA@GCPP NPs and siRNA@GCLPP NPs, the liver (alanine aminotransferase (ALT) and aspartate aminotransferase (AST)) and kidney biomarkers (BUN (blood urea nitrogen)) were measured to determine the systemic toxicity. Repeated inhalation administration of si*KRAS*-loaded NPs (both nontargeted GCPP NPs and targeted GCLPP NPs) were well-tolerated in mice as indicated by no distinguishable changes in organ coefficient, serum liver enzyme levels, and liver histology (Figure 5A−C). However, mild liver toxicity was detected by elevated organ coefficient, serum ALT and AST, and increased inflammation in liver histology *via* repeated IV injection, suggesting that systemic administration of *KRAS* inhibitors might induce liver toxicity. Note that this present study is dedicated to exploring the potential of inhalable siRNA nanotherapeutics for the treatment of *KRAS*-mutant NSCLC. It has been previously reported that less than 20% of the administered drug reaches the lungs through inhalation.[46−48] Despite the potential loss in siRNA therapeutics reaching the lung during inhalation administration, the data reported here indicate that inhaled si*KRAS*@GCLPP NPs still exhibit potent tumor growth inhibition, comparable to the antitumor efficacy of IV-delivered siRNA nanotherapeutics. Additionally, we observed fewer side effects associated with the inhaled si*KRAS*@GCLPP NPs, as evidenced by liver parameters, liver organ coefficient, and histology.

This present study focuses on establishing a proof-of-concept for the design and evaluation of a novel inhalable siRNA nanotherapeutic for the treatment of KRAS-mutant NSCLC, which aims to provide a treatment option against the highly prevalent *KRAS*-driven lung cancers. It is worth noting that *KRAS*-mutant lung cancers exhibit high heterogeneity, and the specific type and comutational signatures can influence tumor biology and response to therapy, as highlighted in previously reported studies.[49,50] In the future, we will explore combination treatment strategies, including chemotherapy and immune checkpoint inhibitors, to further improve the antitumor efficacy of inhaled siRNA-based therapies.

3. CONCLUSIONS

In this work, we show that nebulized gene delivery of GCLPP NPs is safe, specific, and self-stable *via* the inhalation route. si*KRAS*@GCLPP NPs not only showed stable high transfection, clathrin-mediated endocytosis, and effective escape into the cytoplasm, efficiently ablating the targets and their downstream pathways at low concentrations *in vitro*, but also displayed tumor-targeting efficacy in an orthotopic mouse model of human *KRAS*-mutant lung cancer. The present study suggests that inhaled si*KRAS*@GCLPP NPs can deliver equivalent effectiveness compared to intravenous injected (IV) NPs while reducing the adverse effects associated with systemic administration. This novel nanoparticle-based tumor-targeting technology provides proof-of-concept for precision gene therapy of lung cancers and opens new avenues for the treatment of not only *KRAS*-mutant lung cancers but also other lung-related disorders as well.

4. EXPERIMENTAL SECTION

4.1. Synthesis of Cationic Lipid Compound. The cationic lipid-like compound G0-C14 was synthesized with slight modification as described before.[34] Briefly, 1,2 epoxytetradecane was mixed with a PAMAM dendrimer G0 at a molar ratio of 5:1. Substoichiometric amounts of 1,2 epoxytetradecane were added to increase the proportion of products with three less tails than the total possible for a given amine monomer. The mixture was reacted under vigorous stirring at 90 °C for 48 h.

4.2. Synthesis of LHRH-PLGA-PEG. Copolymer PLGA-PEG was synthesized by the amide coupling of maleimide-PEG-NH_2 to PLGA-NHS in methylene chloride.

[D-Lys6]-LHRH decapeptide (Gln-His-Trp-Ser-Tyr-DLys(D-Cys)-Leu-Arg-Pro-NHEt) was purchased from Jiang su Zhong ke hua yao Biotech Ltd. LHRH, which has a reactive amino group only on the side chain of the lysine at position 6, was reacted with 1 equiv of PLGA-PEG in anhydrous dimethylformamide (DMF) at 37 °C for 48 h, and 10 equiv of triethylamine was added every 24 h. After the reaction, the concentrated solution was then dropped to iced methanol to form a white precipitation. The precipitation was washed twice with methanol, and the final product was dried in a desiccator.

For labeling the shell of nanoparticles, PLGA-PEG-Cy5.5 was synthesized as described before.[6−8] Briefly, PLGA was dissolved in dry dichloromethane (DCM). 1-Ethyl-3-[3-dimethylaminopropyl] carbodiimide (EDC)·HCl dissolved in dry DCM and NHS dissolved in anhydrous dimethyl sulfoxide (DMSO) were added in sequence. The solution was stirred at room temperature for 2 h. PLGA-NHS was obtained by precipitation in cold methanol/diethyl ether, further washed two times, and dried by rotary evaporation. PLGA-NHS was dissolved in dry DCM and subsequently, NH2-PEG-Cy5.5 was dissolved in the solution. *N*,*N*-Diisopropylethylamine (DIPEA) was added, and the mixture was stirred at room temperature for 48 h. PLGA-PEG-Cy5.5 (PP-Cy5.5) was obtained by precipitation in methanol/diethyl ether, washed three times by methanol/diethyl ether, and finally vacuum dried to remove the solvent.

4.3. siRNA. siRNAs targeting *KRAS* were synthesized by Biosyntech. The siRNA sequences are as follows: si*KRAS*-1 sense (5′-3′) UGAAUUAGCUGUAUCGUCAAGG, antisense (5′-3′) UUGACGAUACAGCUAAUUCAUA; si*KRAS*-2 sense (5′-3′) ACUGUACUCCUCUUGACCUGCU, antisense (5′-3′) CAGGUCAAGAGGAGUACAGUUA. For Cy7-si*KRAS*, the Cy7 was labeled in the 5′ cap of si*KRAS*-2 sequence.

4.4. Characterization of siRNA Loading Efficiency and Complexation Ability of G0-C14. Naked siRNAs complexed with G0-C14 in varying mass ratios from 1:1 to 1:40 were incubated with a mixture solvent containing DEPC water/DMF (v/v = 1:4) for 30 min. After mixing with a loading buffer, the same volumes of samples were run into a 1% agarose gel stained with gel red for 15 min at 120 V. Then, the gel was imaged under ultraviolet (ChemiDoc MP, Bio-Rad).

4.5. Preparation of siRNA@GCPP NPs and siRNA@GCLPP NPs. We used a self-assembly method to prepare all nanoparticles. Briefly, G0-C14, PLGA-PEG, and LHRH-PLGA-PEG, were dissolved separately in DMF at concentrations of 10 mg/mL. G0-C14 and PLGA-PEG and G0-C14 and LHRH-PLGE-PEG were mixed in 1:1 weight ratio in a tube. siRNA (1 mg/mL) in DNase/RNase-free water was mixed into G0-C14-PLGA-PEG or G0-C14-LHRH-PLGA-PEG to form nanocomplexes (siRNA:PLGA-PEG/LHRH-PLGA-PEG:G0-C14 = 1:20:20, m/m/m). This solution was then dropped into 0.25% PVA aqueous solution with stirring at 500 rpm for 15 min. Then, the mixture was transferred into Amicon tubes (molecular weight cutoff, 100 kDa; Millipore) and washed three times to remove the organic solvent and free molecules. For labeling the shell of NPs, 10% (mass fraction) PLGA-PEG-Cy5.5 was mixed with PLGA-PEG or LHRH-PLGA-PEG.

4.6. pH-Sensitivity Evaluation. Nanoparticles were prepared by nanoprecipitation as described above. The phosphate buffer was adjusted to 3.0, 4.0, 5.0, 6.0, 7.4, and 9.0. After incubation for 2 h, the size distributions and ζ potentials of siRNA@GCPP NPs and

https://doi.org/10.1021/acsami.3c05007
ACS Appl. Mater. Interfaces 2023, 15, 31273−31284

siRNA@GCLPP NPs were determined by the dynamic light scattering method (Malvern ZS90).

4.7. Physicochemical Characterization of siRNA@GCPP NPs or siRNA@GCLPP NPs. Sizes were measured by a Malvern ZS90 at a detection angle of 90° using the dynamic light scattering (DLS) method. The surface charge of the NPs was determined by DLS. For morphology examination, NPs were stained with 1% uranyl acetate and imaged by a transmission electron microscope (Tecnai G2 Spirit BioTWIN, FEI company) at 120 kV.

4.8. Transfection Efficiency of Nanoparticles in Mouse Primary Nasal Mucosal Epithelial Cells. Nasal mucosal epithelial cells from female nu/nu mice were extracted and cultured using a two-step enzymatic digestion method.[51] The fresh nasal septum and the nasal mucosa of the lateral wall of the nasal cavity were taken from the mice with micro tweezers. Then, tissues were washed with precooled sterile PBS containing 1% penicillin−streptomycin antibiotic (Servicebio) 4 times and then rinsed once with HBSS. Next, pieces of tissues were added in 0.1% collagenase type I at 37 °C for 10 min, digesting the collagen connection part in the tissue and gently separating the epithelial cells. 10% fetal bovine serum (FBS, GIBICO) was added to stop the digestion, and the supernatant was removed. 0.25% Trypsin was added and incubated at 37 °C for 2 h to separate the tightly adhered epithelial cells in the tissue, and 10% FBS was used to stop the digestion. After filtering through a 40 μm mesh, the cells were centrifuged at 1000 rpm/min for 10 min, and the precipitate was washed with HBSS. The cells were cultured with DMEM containing 10% FBS and 1% penicillin−streptomycin antibiotic and 25 ng/mL epidermal growth factor (EGF) and then transferred to a 12-well plate. After about 10 days, the cells showed a long spindle shape and covered the entire well plate.

Cy7-cap 5′-labeled siRNA was used to prepare GCP, GCPP, and GCLPP NPs and were transfected into well plates (1.5 μg/mL). The transfection efficiency of positive $Cy7^+$ cells was determined by flow cytometry (BD, Fortessa).

4.9. Cell Culture. Human non-small-cell lung carcinoma (NSCLC) with $KRAS^{G12S}$ muted and the LHRH-receptor-positive cell line A549 was purchased from American Type Culture Collection (ATCC).[52] A549 cells were cultured in DMEM supplemented with 10% FBS and 1% penicillin−streptomycin antibiotic (Thermo Fisher Scientific). Cell culture and biological experiments were performed at 37 °C in 5% CO_2 condition. The A549-Luc cell line was purchased from Ningbo MingZhou Biotechnology Co., Ltd. To maintain A549-Luc cells, 3 μg/mL puromycin was added to the medium. Luciferase expression was analyzed by Bright-Glo luciferase assay (Promega).

4.10. Cellular Uptake and Endosomal Escape of siRNA@GCLPP NPs. Hoechst 33342, Lysotracker Green, and Cy7-siRNA were used to detect the subcellular localization and intracellular trafficking *in vitro*. 2×10^5 A549 cells were seeded into 35 mm glass bottom dishes. After incubation overnight, cells were transfected with 1 μg siRNA/mL Cy7-siRNA@GCLPP NPs in serum-free medium. 4 h post-transfection, the treated cells were washed three times with PBS and cultured with a complete medium. For staining endosome/lysosome and nuclei, cells were cultured with DMEM containing Lysotracker Green (Beyotime) and Hoechst 33342 (Beyotime) were used and incubated for 20 min, and then imaged by a confocal microscope (TCS SP8, Leica). For flow cytometry (BD, Fortessa), the cells were collected and analyzed by Flowjo as described above.

4.11. Mechanism of Cellular Uptake and Endosomal Escape of siRNA@GCLPP NPs. 24-well plates were used to seed A549 cells at a density of 5×10^5 cells per well. After incubation overnight, the cells were pretreated for 30 min in serum-free medium containing inhibitors. Filipin (1 μg/mL), chlorpromazine (10 μg/mL), EIPA (10 μg/mL), and Baf A1 (200 nM) were used to block caveolae-mediated endocytosis, clathrin-mediated endocytosis, micropinocytosis, and intracellular proton-pump effect inhibitors, respectively. The cells were then transfected with Cy7-siRNA@GCLPP NPs at a siRNA concentration of 1 μg/mL. After 4 h, the cells were collected and checked by flow cytometry (BD, Fortessa), and data were analyzed by Flowjo.

4.12. Western Blot. Protein extracts were collected using RIPA lysis buffer (1% NP-40, 0.5% deoxycholate, 0.1% SDS, Beyotime) supplemented with protease inhibitor cocktail (MCE). The cell lysate was then centrifuged at 12,000 rpm for 10 min, and the protein concentration was measured by bicinchoninic acid (BCA) protein assay kit (Beyotime). An equal amount of protein (10 μL) per lane was fractionated on 8 or 10% SDS polyacrylamide gel. After electrophoresis, the gels were transferred into a poly(vinylidene fluoride) (PVDF) membrane and then blocked with 5% bovine serum albumin for 1 h at room temperature. Then, the membranes were incubated for 24 h at 4 °C with a dilution of primary antibodies. After four washes with TBST, membranes were incubated with horseradish peroxidase (HRP)-conjugated secondary antibodies at room temperature for 1 h and subsequently processed for enhanced chemiluminescence (ECL) detection and exposed using ChemiDoc MP (Bio-Rad), pERK1/2 (CST, #4695), ERK1/2 (CST, #4370), *KRAS* (Abclonal, #A1190), AKT (Absin, #abs131788), pAKT (Absin, #abs130002), and GAPDH (Servicebio, #GB12002).

4.13. Cell Death Test. Cell death was assessed using the lactate dehydrogenase (LDH) (Roche) kit, according to the manufacturer's instructions. Absorbances at 492 nm were measured. 2% Triton-X served as the positive control.

4.14. Animals and Lung Cancer Model. All animal experiments were performed according to the Guide for the Care and Use of Laboratory Animals, as adopted and promulgated by the National Institutes of Health, and were approved by the Ethics Committee of Shanghai Jiao Tong University. Female nu/nu mice were purchased from Zhejiang Vital River Laboratory Animal Technologies Co., Ltd (Zhejiang, China). An orthotopic lung cancer mouse model was established by intratracheal instillation of A549-Luc cancer cells as reported.[53,54] In brief, A549-Luc cancer cells (6×10^6 per mouse) were resuspended in 0.1 mL of DMEM containing 20% FBS and mixed with 5 μM EDTA, which was used to allow better tumor engraftment as a slight disruption of the pulmonary epithelium or the surfactant layer.[55] The cancer cell mixtures were administered to the murine lung through a catheter. The progression of tumor growth was monitored using a bioluminescent microscope (IVIS spectrum, PerkinElmer). D-Luciferin potassium salt (150 mg/kg) was intraperitoneally administered 10−15 min before imaging. Mice were anesthetized with isoflurane during imaging procedures.

4.15. Intravital Pulmonary Imaging and Image Processing. All of the intravital lung imaging experiments were supported by IVIM Technology according to institutional and national guidelines.

For intravital imaging, an intravital video-rate laser scanning two-photon microscope (IVM-MS, IVIM technology) was utilized to visualize the inhaled NPs within the lung. Mice were inhaled with Cy5.5-GCLPP NPs at an siRNA single dose of 0.8 mg/kg. FITC-dextran dye (molecular weight 2M Da, Sigma-Aldrich) 25 mg/kg body weight was injected immediately *via* the tail vein. Next, the mice were anesthetized by intraperitoneal injection of 1% pentobarbital sodium at a dose of 10 mL/kg body weight. Then, the mice were ventilated with an inspiratory pressure of 24−30 mmHg, a respiratory rate of 120−130 breaths per minute, and a positive-end expiratory pressure of 2 cm H_2O by using a mouse ventilator (RV-01, Kent Scientific). The body temperature of the mouse was maintained at 37 °C by using the 4CH body and tissue temperature control module (IVM Temp Module, IVIM Technology) integrated into the two-photon microscope. Mice were positioned in right lateral decubitus, followed by dissection of left thoracotomy. Skin and muscle were dissected until the exposure of the rib, and then, an incision was made between the 3rd and 4th rib to expose the pleura. After thoracotomy, the pulmonary imaging window (IVIM Lung Imaging Chamber Set, IVIM technology) optimized for the intravital lung imaging was applied to the surface of the lung. The negative suction pressure of 20−30 mmHg provided by a pump and a regulator (NVC 2300a, EYELA) was applied *via* a tube connected to the imaging window.[56,57]

All image processing was performed using ImageJ and plotting track displacement was conducted using TrackMate.[58]

4.16. Targeting Efficiency of siRNA@GCPP NPs and siRNA@GCLPP NPs in the Orthotopic Lung Cancer Mouse Model. For

https://doi.org/10.1021/acsami.3c05007
ACS Appl. Mater. Interfaces 2023, 15, 31273−31284

this study, the A549-Luc orthotopic lung cancer mouse model received Cy5.5-labeled shell of si*KRAS*@GCPP NPs and Cy5.5-labeled shell of si*KRAS*@GCLPP NPs *via* the tail vein or nose-only inhalation at an siRNA single dose of 0.8 mg/kg (n = 3). Aerogen Solo was used as a nebulizer and was connected to nose-only exposure chambers (made by Shanghai Tow Intelligent Technology Co., Ltd.). Two hours later, organs were collected and imaged with the IVIS spectrum (PerkinElmer). An overlap ratio between tumor signals and fluorescence signals was calculated using ImageJ software.

For the flow cytometry study, lungs were minced and incubated for 1 h at 37 °C in PBS buffer containing 0.92 M HEPES, 201.3 U/mL collagenase I (Sigma), 566.1 U/mL collagenase XI (Sigma), and 50.3 U/mL DNase I (Sigma). Digested tissue was filtered through a 70 μm mesh treated with red blood cell lysis buffer for 5 min. The suspension was centrifuged at 400 G, and pellets were resuspended in PBS containing 0.5% BSA, and filtered through a 40 μm mesh. The cell suspension was centrifugated again; pellets were resuspended and then incubated for 30 min at 4 °C with antibodies against epithelial (EpCAM-AF647), endothelial and A549 cells (CD31-BV421), and immune (CD45-PE) cell markers at a 1:300 dilution. The cells were then analyzed by flow cytometry (BD, Fortessa).

4.17. *In Vivo* Therapeutic Efficacy of si*KRAS*@GCLPP NPs in the Orthotopic Lung Cancer Mouse Model. Four to six weeks post-tumor implantation, mice were randomly divided into four groups: Control (n = 7), si*KRAS*@GCPP NP inhalation (n = 5), si*KRAS*@GCPP NP inhalation (n = 6), and si*KRAS*@GCPP NP injection (n = 5). Mice were administered at a si*KRAS* dose of 0.8 mg/kg body weight at days 0, 4, 8, 11, 15, 19, 22, and 26. Aerogen Solo was used as a nebulizer and was connected to nose-only exposure chambers (made by Shanghai Tow Intelligent Technology Co., Ltd). Around 1 mL/mouse solution was loaded in the nebulizer and unanesthetized animals were placed in the sealed chamber and exposed to aerosol at an airflow rate of 5 L/min for 20 min. The volume for intravenous injection was 0.2 mL per mouse. Animal body weight was monitored during the treatment period. After the treatment on day 27, blood was collected *via* the suborbital venous plexus for biological evaluation. Then, all mice were anesthetized with isoflurane and euthanized. The lung with tumors was imaged by IVIM as an antitumor activity marker. Whole lungs were excised and washed in saline and imaged and then fixed in 10% formalin in PBS for 24 h for histological examination. Serum alanine aminotransferase (ALT), aspartate aminotransferase (AST), and blood urea nitrogen (BUN) were measured by commercial kits according to the manufacturer's instructions (Nanjing Jiancheng Bioengineering Institute).

4.18. Histological Examination and Immunohistochemistry. Whole lung tissues were fixed with 10% formalin, and the max tissue area was sectioned to 5 μm thick slices after staining with hematoxylin and eosin (H&E). For immunohistochemistry, paraffin-embedded sections were used after a microwave-based antigen retrieval technique and stained with anti-*KRAS* antibody (Abclonal, #A1190) or anti-Ki67 antibody (Abclonal, #A2094) at 1:200 dilution, respectively, under a standard protocol. The slides were examined by using a light microscope (BX53, Olympus). The tumor numbers and tumor relative areas (tumor area/ whole tissue area) were analyzed by ImageJ software.

4.19. Statistical Analysis. The experimental results were analyzed using one-way analysis of variance or unpaired two-tailed t-test (GraphPad Prism 7, GraphPad Software Inc., La Jolla, CA) to determine differences between control and treated groups, and the data were shown as means ± standard error of the mean. Values with $p < 0.05$ were considered significant.

■ ASSOCIATED CONTENT

Supporting Information

The Supporting Information is available free of charge at https://pubs.acs.org/doi/10.1021/acsami.3c05007.

Synthesis of PLGA-PEG-LHRH, screening of si*KRAS* sequences *via* RT-PCR, evaluation of the hemolysis of siRNA@GCLPP NPs, and the biodistribution of GCLPP NPs encapsulating Cy7-labeled si*KRAS* (termed Cy7-si*KRAS*@GCLPP NPs) in other organs following inhalation (PDF)

■ AUTHOR INFORMATION

Corresponding Authors

Xiaoyang Xu − *Department of Chemical and Materials Engineering, New Jersey Institute of Technology, Newark, New Jersey 07102, United States; Department of Biomedical Engineering, New Jersey Institute of Technology, Newark, New Jersey 07102, United States;* orcid.org/0000-0002-1634-3329; Email: xiaoyang.xu@njit.edu

Xue-Qing Zhang − *Shanghai Frontiers Science Center of Drug Target Identification and Delivery, School of School of Pharmacy, Shanghai Jiao Tong University, Shanghai 200240, China; National Key Laboratory of Innovative Immunotherapy, Shanghai Jiao Tong University, Shanghai 200240, China;* orcid.org/0000-0002-4954-2586; Email: xueqingzhang@sjtu.edu.cn

Authors

Guolin Zhao − *Shanghai Frontiers Science Center of Drug Target Identification and Delivery, School of School of Pharmacy, Shanghai Jiao Tong University, Shanghai 200240, China; National Key Laboratory of Innovative Immunotherapy, Shanghai Jiao Tong University, Shanghai 200240, China*

William Ho − *Department of Chemical and Materials Engineering, New Jersey Institute of Technology, Newark, New Jersey 07102, United States*

Jinxian Chu − *Shanghai Frontiers Science Center of Drug Target Identification and Delivery, School of School of Pharmacy, Shanghai Jiao Tong University, Shanghai 200240, China; National Key Laboratory of Innovative Immunotherapy, Shanghai Jiao Tong University, Shanghai 200240, China*

Xiaojian Xiong − *Shanghai Frontiers Science Center of Drug Target Identification and Delivery, School of School of Pharmacy, Shanghai Jiao Tong University, Shanghai 200240, China; National Key Laboratory of Innovative Immunotherapy, Shanghai Jiao Tong University, Shanghai 200240, China*

Bin Hu − *Shanghai Frontiers Science Center of Drug Target Identification and Delivery, School of School of Pharmacy, Shanghai Jiao Tong University, Shanghai 200240, China; National Key Laboratory of Innovative Immunotherapy, Shanghai Jiao Tong University, Shanghai 200240, China*

Kofi Oti Boakye-Yiadom − *Shanghai Frontiers Science Center of Drug Target Identification and Delivery, School of School of Pharmacy, Shanghai Jiao Tong University, Shanghai 200240, China; National Key Laboratory of Innovative Immunotherapy, Shanghai Jiao Tong University, Shanghai 200240, China*

Complete contact information is available at: https://pubs.acs.org/10.1021/acsami.3c05007

Author Contributions

X.-Q.Z., X.Xu, and G.Z. conceived and designed the experiments. G.Z. performed most of the experiments. J.C., X.X., B.H., and K.O.B.-Y. assisted with *in vivo* experiments. G.Z., X.-Q.Z., X.Xu, and W.H. wrote the manuscript. All authors have given approval to the final version of the manuscript.

https://doi.org/10.1021/acsami.3c05007
ACS Appl. Mater. Interfaces 2023, 15, 31273−31284

Notes

The authors declare no competing financial interest.

■ ACKNOWLEDGMENTS

X.-Q.Z. acknowledges funding from the "Open Competition to Select the Best Candidates" Key Technology Program for Nucleic Acid Drugs of NCTIB (Grant No. NCTIB2022HS02002), the Natural Science Foundation of Shanghai (23ZR1427600), Shanghai Jiao Tong University Scientific and Technological Innovation Funds (2019TPA10), Foundation of National Facility for Translational Medicine (Shanghai) (TMSK-2020-008), and the Interdisciplinary Program of Shanghai Jiao Tong University [project number ZH2018ZDA36 (19X190020006)]. X.Xu acknowledges support from the National Science Foundation (2001606), and the Gustavus and Louise Pfeiffer Research Foundation Award.

■ ABBREVIATIONS

siRNA, small-interfering RNA
KRAS, Kirsten rat sarcoma
NSCLC, non-small-cell lung cancer
RNAi, RNA interference
LHRH, luteinizing hormone-releasing hormone
Baf A1, bafilomycin A1
MAPK, mitogen-activated protein kinases
PI3K, phosphatidylinositol 3-kinase
BLI, lung bioluminescence imaging
IHC, immunohistochemistry
ALT, alanine aminotransferase
AST, aspartate aminotransferase
BUN, blood urea nitrogen
MFI, mean fluorescence intensity

■ REFERENCES

(1) Sung, H.; Ferlay, J.; Siegel, R. L.; Laversanne, M.; Soerjomataram, I.; Jemal, A.; Bray, F. Global Cancer Statistics 2020: GLOBOCAN Estimates of Incidence and Mortality Worldwide for 36 Cancers in 185 Countries. *Ca-Cancer J. Clin.* **2021**, *71*, 209−249. From NLM.

(2) Oudkerk, M.; Liu, S.; Heuvelmans, M. A.; Walter, J. E.; Field, J. K. Lung cancer LDCT screening and mortality reduction - evidence, pitfalls and future perspectives. *Nat. Rev. Clin. Oncol.* **2021**, *18*, 135−151. From NLM.

(3) Hunter, J. C.; Manandhar, A.; Carrasco, M. A.; Gurbani, D.; Gondi, S.; Westover, K. D. Biochemical and Structural Analysis of Common Cancer-Associated KRAS Mutations. *Mol. Cancer Res.* **2015**, *13*, 1325−1335. From NLM.

(4) Chen, Q.; Gao, M.; Li, Z.; Xiao, Y.; Bai, X.; Boakye-Yiadom, K. O.; Xu, X.; Zhang, X. Q. Biodegradable nanoparticles decorated with different carbohydrates for efficient macrophage-targeted gene therapy. *J. Controlled Release* **2020**, *323*, 179−190. From NLM.

(5) Passiglia, F.; Malapelle, U.; Del Re, M.; Righi, L.; Pagni, F.; Furlan, D.; Danesi, R.; Troncone, G.; Novello, S. KRAS inhibition in non-small cell lung cancer: Past failures, new findings and upcoming challenges. *Eur. J. Cancer* **2020**, *137*, 57−68. From NLM.

(6) Chin, L.; Tam, A.; Pomerantz, J.; Wong, M.; Holash, J.; Bardeesy, N.; Shen, Q.; O'Hagan, R.; Pantginis, J.; Zhou, H.; et al. Essential role for oncogenic Ras in tumour maintenance. *Nature* **1999**, *400*, 468−472. From NLM.

(7) Fisher, G. H.; Wellen, S. L.; Klimstra, D.; Lenczowski, J. M.; Tichelaar, J. W.; Lizak, M. J.; Whitsett, J. A.; Koretsky, A.; Varmus, H. E. Induction and apoptotic regression of lung adenocarcinomas by regulation of a K-Ras transgene in the presence and absence of tumor suppressor genes. *Genes Dev.* **2001**, *15*, 3249−3262. From NLM.

(8) Collins, M. A.; Bednar, F.; Zhang, Y.; Brisset, J. C.; Galbán, S.; Galbán, C. J.; Rakshit, S.; Flannagan, K. S.; Adsay, N. V.; Pasca di Magliano, M. Oncogenic Kras is required for both the initiation and maintenance of pancreatic cancer in mice. *J. Clin. Invest.* **2012**, *122*, 639−653. From NLM.

(9) Chow, M. Y. T.; Chang, R. Y. K.; Chan, H. K. Inhalation delivery technology for genome-editing of respiratory diseases. *Adv. Drug Delivery Rev.* **2021**, *168*, 217−228. From NLM.

(10) Patel, A. K.; Kaczmarek, J. C.; Bose, S.; Kauffman, K. J.; Mir, F.; Heartlein, M. W.; DeRosa, F.; Langer, R.; Anderson, D. G. Inhaled Nanoformulated mRNA Polyplexes for Protein Production in Lung Epithelium. *Adv. Mater.* **2019**, *31*, No. e1805116. From NLM.

(11) Jin, Q.; Zhu, W.; Zhu, J.; Zhu, J.; Shen, J.; Liu, Z.; Yang, Y.; Chen, Q. Nanoparticle-Mediated Delivery of Inhaled Immunotherapeutics for Treating Lung Metastasis. *Adv. Mater.* **2021**, *33*, No. e2007557. From NLM.

(12) Dondi, D.; Limonta, P.; Moretti, R. M.; Marelli, M. M.; Garattini, E.; Motta, M. Antiproliferative effects of luteinizing hormone-releasing hormone (LHRH) agonists on human androgen-independent prostate cancer cell line DU 145: evidence for an autocrine-inhibitory LHRH loop. *Cancer Res.* **1994**, *54*, 4091−4095. From NLM.

(13) Emons, G.; Ortmann, O.; Schulz, K. D.; Schally, A. V. Growth-inhibitory actions of analogues of Luteinizing Hormone Releasing Hormone on tumor cells. *Trends Endocrinol. Metab.* **1997**, *8*, 355−362. From NLM.

(14) Qayum, A.; Gullick, W.; Clayton, R. C.; Sikora, K.; Waxman, J. The effects of gonadotrophin releasing hormone analogues in prostate cancer are mediated through specific tumour receptors. *Br. J. Cancer* **1990**, *62*, 96−99. From NLM.

(15) Klahn, P.; Fetz, V.; Ritter, A.; Collisi, W.; Hinkelmann, B.; Arnold, T.; Tegge, W.; Rox, K.; Hüttel, S.; Mohr, K. I.; et al. The nuclear export inhibitor aminoratjadone is a potent effector in extracellular-targeted drug conjugates. *Chem. Sci.* **2019**, *10*, 5197−5210. From NLM.

(16) Xue, J. Y.; Zhao, Y.; Aronowitz, J.; Mai, T. T.; Vides, A.; Qeriqi, B.; Kim, D.; Li, C.; de Stanchina, E.; Mazutis, L.; et al. Rapid non-uniform adaptation to conformation-specific KRAS(G12C) inhibition. *Nature* **2020**, *577*, 421−425. From NLM.

(17) Zhao, Y.; Murciano-Goroff, Y. R.; Xue, J. Y.; Ang, A.; Lucas, J.; Mai, T. T.; Da Cruz Paula, A. F.; Saiki, A. Y.; Mohn, D.; Achanta, P.; et al. Diverse alterations associated with resistance to KRAS(G12C) inhibition. *Nature* **2021**, *599*, 679−683. From NLM.

(18) Ross, S. J.; Revenko, A. S.; Hanson, L. L.; Ellston, R.; Staniszewska, A.; Whalley, N.; Pandey, S. K.; Revill, M.; Rooney, C.; Buckett, L. K.; et al. Targeting KRAS-dependent tumors with AZD4785, a high-affinity therapeutic antisense oligonucleotide inhibitor of KRAS. *Sci. Transl. Med.* **2017**, *9*, No. eaal5253. From NLM.

(19) Yang, H.; Liang, S. Q.; Schmid, R. A.; Peng, R. W. New Horizons in KRAS-Mutant Lung Cancer: Dawn After Darkness. *Front. Oncol.* **2019**, *9*, No. 953. From NLM.

(20) Liu, P.; Wang, Y.; Li, X. Targeting the untargetable KRAS in cancer therapy. *Acta Pharm. Sin. B* **2019**, *9*, 871−879. From NLM.

(21) Friedlaender, A.; Drilon, A.; Weiss, G. J.; Banna, G. L.; Addeo, A. KRAS as a druggable target in NSCLC: Rising like a phoenix after decades of development failures. *Cancer Treat. Rev.* **2020**, *85*, No. 101978. From NLM.

(22) Thein, K. Z.; Biter, A. B.; Hong, D. S. Therapeutics Targeting Mutant KRAS. *Annu. Rev. Med.* **2021**, *72*, 349−364. From NLM.

(23) Yuan, T. L.; Fellmann, C.; Lee, C. S.; Ritchie, C. D.; Thapar, V.; Lee, L. C.; Hsu, D. J.; Grace, D.; Carver, J. O.; Zuber, J.; et al. Development of siRNA payloads to target KRAS-mutant cancer. *Cancer Discovery* **2014**, *4*, 1182−1197. From NLM.

(24) Zorde Khvalevsky, E.; Gabai, R.; Rachmut, I. H.; Horwitz, E.; Brunschwig, Z.; Orbach, A.; Shemi, A.; Golan, T.; Domb, A. J.; Yavin, E.; et al. Mutant KRAS is a druggable target for pancreatic cancer. *Proc. Natl. Acad. Sci. U.S.A.* **2013**, *110*, 20723−20728. From NLM.

https://doi.org/10.1021/acsami.3c05007
ACS Appl. Mater. Interfaces 2023, 15, 31273−31284

(25) Wang, X. L.; Ramusovic, S.; Nguyen, T.; Lu, Z. R. Novel polymerizable surfactants with pH-sensitive amphiphilicity and cell membrane disruption for efficient siRNA delivery. *Bioconjugate Chem.* **2007**, *18*, 2169−2177.
(26) Malamas, A. S.; Gujrati, M.; Kummitha, C. M.; Xu, R.; Lu, Z. R. Design and evaluation of new pH-sensitive amphiphilic cationic lipids for siRNA delivery. *J. Controlled Release* **2013**, *171*, 296−307.
(27) Sun, D.; Sun, Z.; Jiang, H.; Vaidya, A. M.; Xin, R.; Ayat, N. R.; Schilb, A. L.; Qiao, P. L.; Han, Z.; Naderi, A.; Lu, Z. R. Synthesis and Evaluation of pH-Sensitive Multifunctional Lipids for Efficient Delivery of CRISPR/Cas9 in Gene Editing. *Bioconjugate Chem.* **2019**, *30*, 667−678.
(28) Abdelaziz, H. M.; Gaber, M.; Abd-Elwakil, M. M.; Mabrouk, M. T.; Elgohary, M. M.; Kamel, N. M.; Kabary, D. M.; Freag, M. S.; Samaha, M. W.; Mortada, S. M.; et al. Inhalable particulate drug delivery systems for lung cancer therapy: Nanoparticles, microparticles, nanocomposites and nanoaggregates. *J. Controlled Release* **2018**, *269*, 374−392.
(29) Thakur, A. K.; Chellappan, D. K.; Dua, K.; Mehta, M.; Satija, S.; Singh, I. Patented therapeutic drug delivery strategies for targeting pulmonary diseases. *Expert Opin. Ther. Pat.* **2020**, *30*, 375−387.
(30) Gujrati, M.; Malamas, A.; Shin, T.; Jin, E.; Sun, Y.; Lu, Z. R. Multifunctional cationic lipid-based nanoparticles facilitate endosomal escape and reduction-triggered cytosolic siRNA release. *Mol. Pharmaceutics* **2014**, *11*, 2734−2744.
(31) Lokugamage, M. P.; Vanover, D.; Beyersdorf, J.; Hatit, M. Z. C.; Rotolo, L.; Echeverri, E. S.; Peck, H. E.; Ni, H.; Yoon, J. K.; Kim, Y.; et al. Optimization of lipid nanoparticles for the delivery of nebulized therapeutic mRNA to the lungs. *Nat. Biomed. Eng.* **2021**, *5*, 1059−1068. From NLM.
(32) Islam, M. A.; Xu, Y.; Tao, W.; Ubellacker, J. M.; Lim, M.; Aum, D.; Lee, G. Y.; Zhou, K.; Zope, H.; Yu, M.; et al. Restoration of tumour-growth suppression in vivo via systemic nanoparticle-mediated delivery of PTEN mRNA. *Nat. Biomed. Eng.* **2018**, *2*, 850−864.
(33) Lin, Y. X.; Wang, Y.; Ding, J.; Jiang, A.; Wang, J.; Yu, M.; Blake, S.; Liu, S.; Bieberich, C. J.; Farokhzad, O. C.; et al. Reactivation of the tumor suppressor PTEN by mRNA nanoparticles enhances antitumor immunity in preclinical models. *Sci. Transl. Med.* **2021**, *13*, No. eaba9772.
(34) Xu, X.; Xie, K.; Zhang, X. Q.; Pridgen, E. M.; Park, G. Y.; Cui, D. S.; Shi, J.; Wu, J.; Kantoff, P. W.; Lippard, S. J.; et al. Enhancing tumor cell response to chemotherapy through nanoparticle-mediated codelivery of siRNA and cisplatin prodrug. *Proc. Natl. Acad. Sci. U.S.A.* **2013**, *110*, 18638−18643. From NLM.
(35) Bai, X.; Zhao, G.; Chen, Q.; Li, Z.; Gao, M.; Ho, W.; Xu, X.; Zhang, X. Q. Inhaled siRNA nanoparticles targeting IL11 inhibit lung fibrosis and improve pulmonary function post-bleomycin challenge. *Sci. Adv.* **2022**, *8*, No. eabn7162. From NLM.
(36) Israel, I.; Elflein, K.; Schirbel, A.; Chen, K.; Samnick, S. A comparison of the monomeric. *Eur. J. Pharm. Sci.* **2021**, *166*, No. 105964.
(37) Huang, Y.; Hong, J.; Zheng, S.; Ding, Y.; Guo, S.; Zhang, H.; Zhang, X.; Du, Q.; Liang, Z. Elimination pathways of systemically delivered siRNA. *Mol. Ther.* **2011**, *19*, 381−385.
(38) Smith, S. A.; Selby, L. I.; Johnston, A. P. R.; Such, G. K. The Endosomal Escape of Nanoparticles: Toward More Efficient Cellular Delivery. *Bioconjugate Chem* **2019**, *30*, 263−272. From NLM.
(39) Mattheolabakis, G.; Ling, D.; Ahmad, G.; Amiji, M. Enhanced Anti-Tumor Efficacy of Lipid-Modified Platinum Derivatives in Combination with Survivin Silencing siRNA in Resistant Non-Small Cell Lung Cancer. *Pharm. Res.* **2016**, *33*, 2943−2953. From NLM.
(40) Cho, W. Y.; Hong, S. H.; Singh, B.; Islam, M. A.; Lee, S.; Lee, A. Y.; Gankhuyag, N.; Kim, J. E.; Yu, K. N.; Kim, K. H.; et al. Suppression of tumor growth in lung cancer xenograft model mice by poly(sorbitol-co-PEI)-mediated delivery of osteopontin siRNA. *Eur. J. Pharm. Biopharm.* **2015**, *94*, 450−462. From NLM.
(41) Biswas, S.; Deshpande, P. P.; Navarro, G.; Dodwadkar, N. S.; Torchilin, V. P. Lipid modified triblock PAMAM-based nanocarriers for siRNA drug co-delivery. *Biomaterials* **2013**, *34*, 1289−1301. From NLM.
(42) Liu, X.; Howard, K. A.; Dong, M.; Andersen, M.; Rahbek, U. L.; Johnsen, M. G.; Hansen, O. C.; Besenbacher, F.; Kjems, J. The influence of polymeric properties on chitosan/siRNA nanoparticle formulation and gene silencing. *Biomaterials* **2007**, *28*, 1280−1288. From NLM.
(43) Sun, C. Y.; Shen, S.; Xu, C. F.; Li, H. J.; Liu, Y.; Cao, Z. T.; Yang, X. Z.; Xia, J. X.; Wang, J. Tumor Acidity-Sensitive Polymeric Vector for Active Targeted siRNA Delivery. *J. Am. Chem. Soc.* **2015**, *137*, 15217−15224. From NLM.
(44) Vert, J. P.; Foveau, N.; Lajaunie, C.; Vandenbrouck, Y. An accurate and interpretable model for siRNA efficacy prediction. *BMC Bioinf.* **2006**, *7*, No. 520. From NLM.
(45) Fellmann, C.; Zuber, J.; McJunkin, K.; Chang, K.; Malone, C. D.; Dickins, R. A.; Xu, Q.; Hengartner, M. O.; Elledge, S. J.; Hannon, G. J.; Lowe, S. Functional identification of optimized RNAi triggers using a massively parallel sensor assay. *Mol. Cell* **2011**, *41*, 733−746. From NLM.
(46) Ganguly, S.; Moolchandani, V.; Roche, J. A.; Shapiro, P. S.; Somaraju, S.; Eddington, N. D.; Dalby, R. N. Phospholipid-induced in vivo particle migration to enhance pulmonary deposition. *J. Aerosol Med. Pulm. Drug Delivery* **2008**, *21*, 343−350.
(47) Patton, J. S. Unlocking the opportunity of tight glycaemic control. Innovative delivery of insulin via the lung. *Diabetes, Obes. Metab.* **2005**, *7*, S5−S8.
(48) Kolanjiyil, A. V.; Kleinstreuer, C. Nanoparticle mass transfer from lung airways to systemic regions–Part I: Whole-lung aerosol dynamics. *J. Biomech. Eng.* **2013**, *135*, No. 121003.
(49) Friedlaender, A.; Drilon, A.; Weiss, G. J.; Banna, G. L.; Addeo, A. KRAS as a druggable target in NSCLC: Rising like a phoenix after decades of development failures. *Cancer Treat. Rev.* **2020**, *85*, No. 101978.
(50) Huang, L.; Guo, Z.; Wang, F.; Fu, L. KRAS mutation: from undruggable to druggable in cancer. *Signal Transduction Targeted Ther.* **2021**, *6*, No. 386.
(51) Davidson, D. J.; Gray, M. A.; Kilanowski, F. M.; Tarran, R.; Randell, S. H.; Sheppard, D. N.; Argent, B. E.; Dorin, J. R. Murine epithelial cells: isolation and culture. *J. Cystic Fibrosis* **2004**, *3*, 59−62. From NLM.
(52) Lu, C.; Huang, T.; Chen, W.; Lu, H. GnRH participates in the self-renewal of A549-derived lung cancer stem-like cells through upregulation of the JNK signaling pathway. *Oncol. Rep.* **2015**, *34*, 244−250. From NLM.
(53) Garbuzenko, O. B.; Kuzmov, A.; Taratula, O.; Pine, S. R.; Minko, T. Strategy to enhance lung cancer treatment by five essential elements: inhalation delivery, nanotechnology, tumor-receptor targeting, chemo- and gene therapy. *Theranostics* **2019**, *9*, 8362−8376. From NLM.
(54) Garbuzenko, O. B.; Saad, M.; Pozharov, V. P.; Reuhl, K. R.; Mainelis, G.; Minko, T. Inhibition of lung tumor growth by complex pulmonary delivery of drugs with oligonucleotides as suppressors of cellular resistance. *Proc. Natl. Acad. Sci. U.S.A.* **2010**, *107*, 10737−10742. From NLM.
(55) March, T. H.; Marron-Terada, P. G.; Belinsky, S. A. Refinement of an orthotopic lung cancer model in the nude rat. *Vet. Pathol.* **2001**, *38*, 483−490. From NLM.
(56) Park, I.; Choe, K.; Seo, H.; Hwang, Y.; Song, E.; Ahn, J.; Hwan Jo, Y.; Kim, P. Intravital imaging of a pulmonary endothelial surface layer in a murine sepsis model. *Biomed Opt Express* **2018**, *9*, 2383−2393. From NLM.
(57) Park, I.; Kim, M.; Choe, K.; Song, E.; Seo, H.; Hwang, Y.; Ahn, J.; Lee, S. H.; Lee, J. H.; Jo, Y. H.; et al. Neutrophils disturb pulmonary microcirculation in sepsis-induced acute lung injury. *Eur. Respir. J.* **2019**, *53*, No. 1800786. From NLM.
(58) Tinevez, J. Y.; Perry, N.; Schindelin, J.; Hoopes, G. M.; Reynolds, G. D.; Laplantine, E.; Bednarek, S. Y.; Shorte, S. L.; Eliceiri, K. W. TrackMate: An open and extensible platform for single-particle tracking. *Methods* **2017**, *115*, 80−90. From NLM.

https://doi.org/10.1021/acsami.3c05007
ACS Appl. Mater. Interfaces 2023, 15, 31273−31284